https://doi.org/10.5194/amt-2020-202
Preprint. Discussion started: 29 June 2020

Atmospheric Measurement Techniques Discussions

On the relationship between wind observation accuracy and the ascending node of sun-synchronous orbit for the Aeolus-type spaceborne Doppler wind lidar

Chuanliang Zhang[1,2], Xuejin Sun[2], Wen Lu[2], Yingni Shi[1], Naiying Dou[1], and Shaohui Li[2]

[1]Mailbox 5111, Beijing 100094, China
[2]College of Meteorology and Oceanography, National University of Defense Technology, Nanjing 211101, China

Corresponding to: Xuejin Sun (xuejin.sun@outlook.com)

Abstract. The launch and operation of first spaceborne Doppler wind lidar (DWL) Aeolus is of great significance in observing global wind field. Aeolus operates on the sun-synchronous dawn-dusk orbit to minimize the negative impact of solar background radiation (SBR) on wind observation accuracy. For that the future spaceborne DWLs may not operate on sun-synchronous dawn-dusk orbits due to their observation purposes, the impact of the local time of ascending node (LTAN) crossing of sun-synchronous orbits on the wind observation accuracy was studied in this paper by proposing two added Aeolus-type spaceborne DWLs operated on the sun-synchronous orbits with LTAN of 15:00 and 12:00 combined with Aeolus. On the two new orbits, the increments of averaged SBR received by the new spaceborne DWLs range from 39 to 56 $mW \cdot m^{-2} \cdot sr^{-1} \cdot nm^{-1}$ under clear skies, which will lead to the increment of averaged wind observation uncertainties from 0.3 to 0.4 m/s in the troposphere and from 0.9 to 1.4 m/s in the stratosphere. Increasing laser pulse energy of the new spaceborne DWLs is used to lower the wind observation uncertainties. Furthermore, a method to quantitatively design the laser pulse energy according to specific accuracy requirements is given in this paper based on the relationship between the signal noise ratio and the uncertainty of response function of Rayleigh channel of Aeolus-type spaceborne DWLs. The laser pulse energy of the two new spaceborne DWLs is set to 80 mJ based on the statistical results according to the method, meanwhile other instrument parameters are the same as those of Aeolus. Based on the parameter proposal, the accuracy of above 85% bins of the new spaceborne DWLs would meet the accuracy requirements of European Space Agency (ESA) for Aeolus, which would improve the forecast results of Numerical Weather Prediction. And the averaged observation uncertainties show the consistence in observation accuracy of the three spaceborne DWLs, which can be used for joint observations.

1 Introduction

The first spaceborne Doppler wind lidar (DWL) mission ADM-Aeolus (ADM, Atmospheric Dynamics Mission) designed by European Space Agency (ESA) was launched successfully on 22 August 2018, which improves people's knowledge on global wind field. Aeolus carries a spaceborne DWL, Atmospheric Laser Doppler Instrument (ALADIN), has been used to make preliminary observations of global wind field since the launch. And the first Numerical Weather Prediction (NWP) experiments show that the assimilated wind observations have significant positive impact in the forecast of wind, humidity and temperature

https://doi.org/10.5194/amt-2020-202
Preprint. Discussion started: 29 June 2020


Atmospheric Measurement Techniques Discussions

at short-range, especially in the tropical troposphere and south hemisphere (Straume *et al.*, 2019). Furthermore, scientists have also designed several possible observation scenarios of future spaceborne DWLs. Considering Aeolus can only realize the observations of single horizontal line-of-sight (LOS) wind components, Ma *et al.*, (2015) and Masutani *et al.*, (2010) proposed a spaceborne DWL concept with two pairs of telescopes (azimuth angles from one pair is 45° and 315°, the other pair is 135° and 225°) using both coherent-detection and direct-detection technology, and ISHII *et al.*, (2017) proposed the spaceborne coherent DWL concept with one pair of telescopes (azimuth angles of 45° and 315°), both of the two observation scenarios can provide the horizontal vector wind. In addition, Marseille et al. (2008) demonstrated that larger observation coverage is more beneficial in the improvement of NWP results in global scale compared to the measurement of horizontal vector wind by proposing several multi-satellites joint observation scenarios with Aeolus-type instruments. However, the observations of horizontal vector wind perform better for NWP results in the region close to the satellite tracks. In short, Aeolus is a demonstration mission which primarily aims to improve NWP and medium-range weather forecast, and there will be more observation scenarios of spaceborne DWLs with different observation purposes launched in the future.

The future spaceborne DWLs may operate on different orbits which should be related to their observation purposes. Aeolus operates on the sun-synchronous, dawn-dusk orbit to minimize the impact of solar background radiation (SBR) on the accuracy of wind observations (Heliere *et al.*, 2002, Baars *et al.*, 2019). The SBR is defined as the top-of-atmosphere (TOA) radiance which directs to the telescopes of spaceborne DWLs, and the solar background noise (SBN) is the photon counts excited by SBR and imaged on the photon detectors (Zhang *et al.*, 2018) which would lower the observation accuracy by Poisson noise (Liu *et al.*, 2006, Hasinoff *et al.*, 2010). The dawn-dusk orbit is an optimal proposal to lower SBR for spaceborne DWLs operating on sun-synchronous orbits. If the future spaceborne DWLs would operate on the sun-synchronous orbits with different local time of ascending node (LTAN) crossing, the received SBR would become larger which would lead to higher uncertainties of wind observations.

According to the technology mechanism of Aeolus, the factors that affect the observations accuracy of spaceborne DWLs include atmospheric heterogeneity, SBR, et al. Aeolus is a direct-detection Doppler wind lidar which sensing winds through Mie channel and Rayleigh channel. Mie channel sensing winds using the laser signal backscattered from aerosol/cloud particles, and Rayleigh channel sensing winds using molecular backscatter signal. Atmospheric heterogeneity mainly affects the wind observations on Mie channel. Sun *et al.*, (2014) indicate that typical values for wind uncertainties on Mie channel in the free troposphere are in the range of 1~1.5 m/s caused by atmospheric heterogeneity, which cannot be easily corrected. And for Rayleigh channel, the uncertainties caused by atmospheric heterogeneity are between 0.2 and 0.6 m/s in the troposphere, which can be largely reduced by scene classification algorithm. SBR mainly affects the observations on Rayleigh channel, and has less impact on the observations in Mie channel (Rennie, 2017). The received SBR of Aeolus ranges from 0 to 169 $mW \cdot m^{-2} \cdot sr^{-1} \cdot nm^{-1}$. Zhang *et al.*, (2019) shows that the mean uncertainties in the wind observation of Aeolus would increase

https://doi.org/10.5194/amt-2020-202
Preprint. Discussion started: 29 June 2020


Atmospheric Measurement Techniques Discussions

by 0.18, 0.69 m/s in the troposphere and stratosphere respectively as 20 $mW \cdot m^{-2} \cdot sr^{-1} \cdot nm^{-1}$ of SBR increases. When the SBR is greater than 80 $mW \cdot m^{-2} \cdot sr^{-1} \cdot nm^{-1}$, the whole profiles of wind observations would be less accurate.

The observations of global wind would improve the results of NWP, however, if the observations of low accuracy are assimilated, the negative impact on NWP results would be introduced (Stoffelen *et al.*, 2005, 2006). According to the accuracy requirements of ESA, the uncertainties of the horizontally projected line-of-sight (HLOS) wind observations in the Planetary Boundary Layer (PBL), free troposphere, and stratosphere should be less than 1, 2, and 3 m/s respectively (Stoffelen et al., 2005). And the latest research also demonstrated that the uncertainty of 1 m/s in PBL, 2.5 m/s in free troposphere, and 3~5 m/s in stratosphere would also allow significant positive impact in NWP results (Straume *et al.*, 2019). The height boundary between the PBL, free troposphere and stratosphere are 2 km and 16 km respectively. In this paper, we assumed that the accuracy of 5 m/s in stratosphere was required. And the troposphere mentioned below specially referred to the free troposphere.

Assuming the future Aeolus-type spaceborne DWLs will operate on the sun-synchronous orbits with different LTAN, the distributions of received SBR and corresponding uncertainties of wind observations caused by SBR were figured out in this paper. The method to lower the uncertainty to specific accuracy level, i.e. to meet the accuracy requirements of ESA, or to reach the similar accuracy level of Aeolus, was also discussed. In general, the only way to reduce the effect of Poisson noise was to capture more signal (Vahlbruch *et al.*, 2008). According to the lidar equation, the following methods can be used to increase return signal energy of spaceborne DWLs: 1) increasing the laser pulse energy; 2) lowering the height of orbits; 3) enlarging the telescope aperture; 4) reducing vertical resolution (Marseille and Stoffelen, 2003). In addition, the orbit height of Aeolus was adjusted from originally designed 400 km to 320 km to increase energy of received signal. In this paper, increasing laser pulse energy was used to lower the uncertainty. The remainder of this paper is organized as follows. The details of the orbits of the three spaceborne DWLs and the Aeolus-type spaceborne DWL simulation system are presented in Sect. 2. Section 3 gives a method to quantitatively design the laser pulse energy of spaceborne DWLs based on specific accuracy requirements. Before that, the relationship between the signal noise ratio (SNR) and the uncertainty of response function of Rayleigh channel is also discussed. In Sect. 4, the preliminary proposal of laser pulse energy of the two new spaceborne DWLs is given using the method mentioned in Sect. 3 based on the global distributions of SBR and wind observation uncertainties, as well as the accuracy requirements for spaceborne DWLs. Sect. 5 presents the summary and conclusions.

2 The sun-synchronous orbits and simulation system of spaceborne DWLs

In general, for sun-synchronous orbits, the spaceborne DWL runs on the dawn-dusk orbit would receive minimum SBR, and the spaceborne DWL runs on the noon-midnight orbit would receive maximum SBR. In order to study the impact of orbit selection on the wind observation accuracy, the spaceborne DWL runs on three sun-synchronous orbits with LTANs of 18:00,

https://doi.org/10.5194/amt-2020-202
Preprint. Discussion started: 29 June 2020

Atmospheric Measurement Techniques Discussions

15:00, and 12:00 respectively were proposed. And the simulation system used to calculate the uncertainty of wind observations was also described.

2.1 The sun-synchronous orbits

The three orbits with LTANs of 18:00, 15:00, and 12:00 are illustrated in Fig.1 (a). Aeolus operates in the sun-synchronous, dawn-dusk orbit with height of 320 km marked in blue. The spaceborne DWL is equipped with a single-perspective telescope, which scanning at 90° with respect to the satellite track, under a slant angle of 35° versus nadir, measuring profiles of HLOS wind components. The other two spaceborne DWLs run in the sun-synchronous orbit with LTANs of 15:00 and 12:00 which are marked in yellow and red lines respectively. The intersection points between laser beam and earth surface are called off-nadir points of which lines are illustrate in Fig. 1(b).

The received SBR of spaceborne DWLs is related to their optical architecture and instrument parameters. The two new spaceborne DWLs are assumed to be Aeolus-type instruments whose instrument parameters the same as those of Aeolus except higher laser pulse energy which aims to improve wind observation accuracy. The number of wind component profiles observed by the joint observation scenario of three spaceborne DWLs is three times the number of Aeolus, which would enlarge observation coverage and largely improve the results of NWP forecasts.

According to the characteristics of sun-synchronous orbits, the local observation time of the spaceborne DWLs focus mostly on about 06:00/18:00, 03:00/15:00, and 00:00/12:00. The shadow area of Fig. 1(b) illustrates the observations in nighttime. Figure 1(b) shows that the solar zenith angle of the observation points of the two new Aeolus-type instruments is low compared to that of Aeolus, and thus lead to larger SBR. The phenomenon also indicates that the sun-synchronous dawn-dusk orbit is the orbit which would receive the minimum SBR compared to the others.

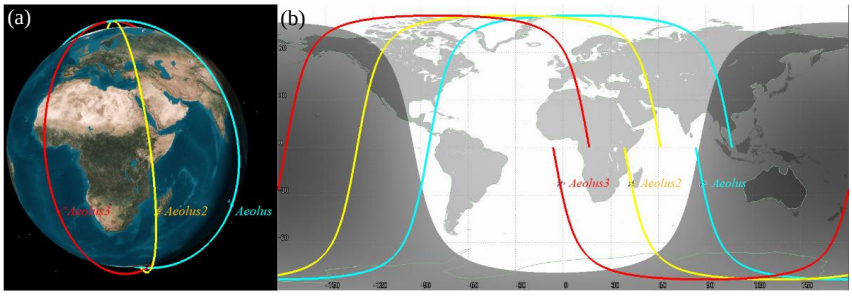

Figure 1. The orbits of the spaceborne DWLs operate on the sun-synchronous orbits with LTAN of 18:00, 15:00, and 12:00, which are marked in blue, yellow, and red respectively. (a) 3D graphics; (b) 2D graphics.

2.2 Spaceborne DWL simulation system

An Aeolus-type spaceborne DWL simulation system was used to retrieve HLOS wind components and calculate observation uncertainties. The simulation system was built according to the optical structure of Aeolus which were consist of laser transmitter, the telescope and front optics, Mie spectrometer, Rayleigh spectrometer, and detection front units (Marseille and

https://doi.org/10.5194/amt-2020-202
Preprint. Discussion started: 29 June 2020


Atmospheric Measurement Techniques Discussions

Stoffelen, 2003 and Paffrath, 2006). Considering that SBR mainly affect the observation accuracy of Rayleigh channel, we focus on the simulation of the wind retrieved method on Rayleigh channel, and assume that the cross-talk effect between Mie channel and Rayleigh channel is negligible. The details of the working principle and instrument parameters of Aeolus used in the simulation system are set according to the Algorithm Theoretical Basis Document (ATBD): ADM-Aeolus Level1B products (Reitebuch *et al.*, 2006), expect the mean altitude of satellite which is set to 320 km, the laser pulse energy which is set to 60 mJ, and the repetition rate of the laser transmitter is set to 50 Hz. In addition, in the simulation system, one observation consists of 50 accumulations (also called as measurements) of 14 shots. Combined with the ground speed of Aeolus of 7.2 km/s, the horizontal resolution of about 100.8 km per observation. The vertical resolutions of retrieved wind are 500 m in the PBL, 1 km in the troposphere, and 2 km in the stratosphere (Marseille et al., 2008).

The input parameters of simulation system included u- and v- components wind, temperature, pressure, aerosol optical properties, and TOA radiance. In this paper, the impacts of SBR on the wind observation accuracy of spaceborne DWLs under cloudy atmosphere were not considered. The first five components are derived from the pseudo-truth global atmospheric condition dataset, which consists of the Ozone Monitoring Instrument (OMI) database (McPeters *et al.*, 2008), including the latitude-averaged profiles of temperature, pressure, and density of ozone, and the lidar climatology of vertical aerosol structure for spaceborne lidar simulation studies (LIVAS) database (Amiridis *et al.*, 2015), which was used to describe aerosol optical properties. The details to derive the global distributions of SBR received by Aeolus-type spaceborne DWLs can refer to (Zhang *et al.*, 2019), which were briefly introduced here. First, the satellite orbit simulation software was required to obtain the positions of the off-nadir points of the spaceborne DWLs. Atmospheric conditions were retrieved from the pseudo-truth databases and spatially interpolated to the off-nadir points. The surface albedo was also needed to generate the TOA radiance, which were derived from the database of lambert-equivalent reflectivity (LER) (Koelemeijer *et al.*, 2003). Then the SBR of off-nadir points was generated by radiative transfer model (RTM) libRadtran with the input of temperature, pressure, aerosol optical properties, and surface albedo (Emde *et al.*, 2016). Once the atmospheric conditions and SBR were input to the simulation system, the HLOS winds and their corresponding uncertainties could be figured out.

3 Methodology

Increasing the laser pulse energy of Aeolus-type spaceborne DWLs was used to lower wind observation uncertainties in this paper. To quantitatively design the laser pulse energy of two new spaceborne DWLs as mentioned in Subsect. 2.1, the steps are as follows: 1) the global distributions of SBR received by the spaceborne DWLs on the three orbits are figured out to compare the SBR received by the two new spaceborne DWLs with that of Aeolus. In this paper, the global distributions of SBR near the summer solstice which range from June 14 to 28 are derived as the SBR in summer and near the winter solstice which ranges from December 15 to 30 are derived as the SBR in winter; 2) the uncertainties of wind observations on Rayleigh

https://doi.org/10.5194/amt-2020-202
Preprint. Discussion started: 29 June 2020


Atmospheric Measurement Techniques Discussions

channel of the three spaceborne DWLs are derived and the uncertainty increments of the two new spaceborne DWLs compared to that of Aeolus are figured out; 3) the relationship between wind observation uncertainty and laser pulse energy is established; 4) the value of laser pulse energy which would lower the uncertainties to required accuracy level is derived based on the relationship established in the step 3).

3.1 Uncertainty of wind observation on Rayleigh channel

The double-edge technique was used to retrieve the HLOS wind components on Rayleigh channel for Aeolus (Flesia and Korb, 1999, Zhang et al., 2014). The study of Tan *et al.*, (2008) shows that the uncertainty on Rayleigh channel is determined by response function, temperature, pressure, and scattering ratio. Lookup table between wind speed and response function, temperature, pressure, scattering ratio was established prior to the launch of Aeolus. In operation mode, the profiles of temperature and pressure are obtained from the European Centre for Medium-Range Weather Forecasts (ECMWF) data assimilation system. The scattering ratio can be derived from the intensity of the signal received by Rayleigh channel and Mie channel (Flamant *et al.*, 2008), which are assumed to be accurate (no uncertainty) in this paper. Once the response function of Rayleigh channel was detected, wind speed would be figured out. The uncertainty of wind observation is estimated as

$$\sigma_{HLOS} = \frac{\partial v_{HLOS}}{\partial R_{ATM}} \sigma_{R_{ATM}} \tag{1}$$

where $\sigma\cdot$ denotes uncertainty, $\partial\cdot$ denotes partial derivative. v_{HLOS} means the HLOS wind component. R_{ATM} means response function of Rayleigh channel which is defined as

$$R_{ATM} = \frac{N_A - N_B}{N_A + N_B} \tag{2}$$

where N_A and N_B are the useful signal detected by Rayleigh channel.

The $\partial v_{HLOS}/\partial R_{ATM}$ is a function of temperature and pressure, which ranges from 420 to 520 m/s upon most occasions, as shown in Fig. 1 of Zhang et al., (2019). The uncertainty of response function is derived from

$$\sigma_{R_{ATM}} = \frac{2}{(N_A + N_B)^2} \sqrt{N_B^2 \sigma_A^2 + N_A^2 \sigma_B^2} \tag{3}$$

where σ_A and σ_B denote the uncertainty of N_A and N_B. Here, N_A and N_B can be obtained using the simulation system of spaceborne DWLs. Taking the SBR and the dark current of spaceborne DWL detectors into account, according to the feature of Poisson noise, the uncertainty in N_A and N_B can be estimated as

$$\sigma_A^2 = N_A + N_{S,A} + N_{noise}^2, \sigma_B^2 = N_B + N_{S,B} + N_{noise}^2 \tag{4}$$

where the $N_{S,A}$ and $N_{S,B}$ are the photon counts which are excited by SBR on Rayleigh channel. N_{noise} denote the dark current of Accumulation Charge Coupled Device (ACCD) on Rayleigh channel.

$N_{S,A}$ and $N_{S,B}$ can be derived using the following method: the SBR can be viewed as the spectrum which follows the uniform distribution of which energy can be obtained using Eq. (5) of Nakajima *et al.*, (1999), and the bandwidth equals to

https://doi.org/10.5194/amt-2020-202
Preprint. Discussion started: 29 June 2020


Atmospheric Measurement Techniques Discussions

that of the interference filter of the Rayleigh channel. $N_{S,A}$ and $N_{S,B}$ can be obtained from the simulation system with the input of the spectrum.

$$S_{SBR} = nE_Q E_O L_S \varphi_R \frac{A_r^2 \cdot \pi}{4} \Delta\lambda \Delta t \quad (5)$$

where S_{SBR} denotes the energy of SBR, n denotes the number of the accumulated laser shots, E_Q and E_O denote the quantum efficiency of the detector on Rayleigh channel, L_S denotes the TOA radiance of the off-nadir point. As to the instrument parameters, φ_R denotes the field of view; A_r denotes the diameter of the telescope; $\Delta\lambda$ denote the bandwidth of the interference filter. Δt denotes the laser detection time which was dependent on the vertical resolution.

3.2 Relationship between uncertainty and laser pulse energy

The laser pulse energy of laser transmitter has an important influence on the uncertainty of wind observation. Provided the atmospheric conditions remain unchanged, the higher the laser energy, the backscattered signal received by the telescope of Aeolus-type instrument will become stronger, and the corresponding Poisson noise will be smaller, which will lower the uncertainty of wind observation. However, due to that the wind observation uncertainty is affected by various factors such as the atmospheric conditions and instrument parameters, the quantitative relationship between laser pulse energy and wind observation uncertainty is not yet derived. In this paper, the method for quantitative derivation of the laser pulse energy according to specific accuracy requirement of wind observation was proposed through the relationship between SNR of Rayleigh channel and uncertainty of response function of Rayleigh channel.

According to the characteristics of Poisson noise, Marseille and Stoffelen, (2003) defined the SNR of Rayleigh channel.

$$SNR_{Ray} = \frac{N_A + N_B}{\sqrt{N_A + N_B + N_{S,A} + N_{S,B} + 2N_{noise}^2}} \quad (6)$$

For the Rayleigh channel of spaceborne DWL, difference between N_A and N_B is not large, especially when the wind speed is close to zero, $N_A \approx N_B$. Based on the assumption that $N_A \approx N_B$, we derived the relationship between the SNR and uncertainty of response function of the Rayleigh channel.

$$\sigma_{R_{ATM}} \approx \frac{1}{SNR_{Ray}} \quad (7)$$

The details of the derivations and proofs are shown in Appendix. Then the uncertainty of wind observation on Rayleigh channel can be estimated as

$$\sigma_{v_{HLOS}} \approx \frac{\partial v_{HLOS}}{\partial R_{ATM}} \cdot \frac{1}{SNR_{Ray}} \quad (8)$$

While increasing the laser pulse energy, the value of $N_A + N_B$ will proportional increase; similarly, $N_{S,A} + N_{S,B}$ will proportional increase with the increase of SBR, which can be written as

$$E_{laser} \propto N_A + N_B, S_{SBR} \propto N_{S,A} + N_{S,B} \quad (9)$$

https://doi.org/10.5194/amt-2020-202
Preprint. Discussion started: 29 June 2020


Atmospheric Measurement Techniques Discussions

According to Eqs. (6) and (8), setting $x = N_A + N_B$, which is in proportion to the energy of laser pulse E_{lasr}; $y = N_{S,A} + N_{S,B}$, which is in proportion to the energy of SBR S_{SBR}, and $z = \sigma_{HLOS}$, $f(T,P) = \partial v_{HLOS}/\partial R_{ATM}$, $C = 2N_{noise}^2$, where T denotes temperature and P denotes pressure, the relationship between x, y, and z can be expressed as

$$z \approx f(T,P)\frac{\sqrt{x+y+C}}{x} \tag{10}$$

Equation (10) can be solved as

$$x \approx \frac{f^2(T,P)+f(T,P)\cdot\sqrt{f^2(T,P)+4z^2(y+C)}}{2z^2} \tag{11}$$

Equation (10) illustrates that the uncertainty is determined by temperature, pressure, variable x, the SBR, and dark noise of the detector. The value of x can be estimated using Eq. (11). Knowing the value of x, the value of laser energy cannot be figured out for that the variable x is dependent on the laser energy and wind speed. However, when the wind speed keeps unchanged, the variable x would be in proportion to the energy of laser pulse E_{laser}. That is to say, if the laser energy increases by several times, the corresponding value of variable x will increase by the same multiples when the HLOS wind speed keeps unchanged. Then the required value of laser energy can be obtained based on the proportional relationship between x and E_{laser}.

3.3 Derivation of laser pulse energy

In Subsect. 3.2 and Appendix, the relationship between laser pulse energy E_{laser} and wind observation uncertainty was established based on some assumption and simplifications. The following methods was used to solve the problem that how much the laser energy could be set to increase the accuracy of the observation of new spaceborne DWLs to the meet specific accuracy requirements.

Firstly, the laser pulse energy of the two new spaceborne DWLs was assumed to be 60 mJ of which parameter are the same as that of Aeolus, the profiles of uncertainty were derived using simulation system based on the global distributions of SBR on the three orbits; secondly, the profiles of variable x at each bin (layer, the concept can refer to Fig. 5 in Tan et al., (2008)) were figured out using Eq. (11), which were set as $x1$. Provided that the accuracy requirements of the two new spaceborne DWLs are to reach the accuracy level of Aeolus, then, the uncertainty of the new spaceborne DWLs were replaced with the uncertainty of Aeolus at the same bins, and the variables of $f(T,P)$, y, and C kept unchanged, the variables x were figured out using Eq. (11), which were set as $x2$; finally, according to the proportional relationship between x and laser energy, $E_{new}/E_{Aeolus} \approx x2/x1$, the required laser pulse energy at each bin could be derived. Therefore, we could determine the laser energy of the two new spaceborne DWLs according to the statistical results.

In the same way, if the accuracy requirements of the two new spaceborne DWLs were to meet the accuracy requirements of ESA, we needed to replace the wind observation uncertainty which were calculated when the laser energy is 60 mJ with the accuracy requirements of ESA when calculating the value of $x2$, and the other steps were the same as above.

https://doi.org/10.5194/amt-2020-202
Preprint. Discussion started: 29 June 2020

Atmospheric Measurement Techniques Discussions

4 Results and discussions

A preliminary result for determining the laser pulse energy of two new spaceborne DWLs was presented in this section. To obtain the laser pulse energy, the global distributions of SBR on the three orbits and the corresponding wind observation uncertainty caused by SBR were calculated, firstly. Then the distributions of required laser energy were obtained according to accuracy requirements based on the method mentioned in Subsect. 3.3. Finally, based on the results, a proposal of determining the laser energy of two new spaceborne DWLs was presented. And the global distributions of wind observation uncertainties of the three spaceborne DWLs were figured out according to the instrument parameter proposal. The details were shown in the following subsections.

4.1 Global distributions of SBR on the three orbits

The SBR received by spaceborne DWLs is mainly determined by instrument parameters and orbits. Global distributions of the SBR received by the spaceborne DWLs run on the three orbits in summer and winter are shown in Fig. 2 based on the instrument parameters of Aeolus and the orbits mentioned in Subsect. 2.1.

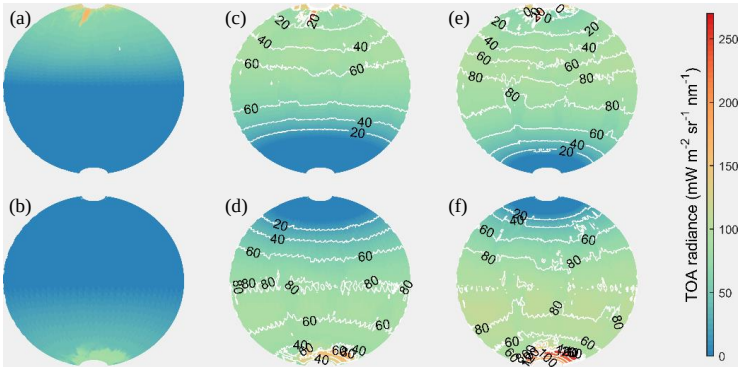

Figure 2. Global distributions of SBR received by spaceborne DWLs operated on the three orbits. The contours in the Figs. (c, e), (d, f) denote the difference between the SBR in Figs. (c, e), (d, f) with the SBR in Figs. (a, b), respectively. Figs. (a, b), (c, d) and (e, f) present the sun-synchronous orbits with LTAN of 18:00, 15:00, and 12:00 respectively, and the upper panels denote the SBR in summer, and the lower panels denote the SBR in winter.

The contours in Fig. 2 demonstrate that the dawn-dusk orbit is an effective solution to minimize SBR received by spaceborne DWL operated on sun-synchronous orbits. While operating on the sun-synchronous dawn-dusk orbit, the SBR of the off-nadir points located in the southern hemisphere is nearly equal to zero in summer, and the SBR of the off-nadir points located in the northern hemisphere is nearly equal to zero in winter. For the two new orbits, there are fewer areas with SBR of zero, mainly located in the regions near the Antarctic and Arctic circles. According to the contours, the ascending order of the values of SBR in the three orbits is dawn-dusk orbit, the orbits with LTAN of 15:00, and that of 12:00 respectively. The closer the LTANs of the orbits to noon, the values and the affected area of SBR will become larger. The differences of SBR received by the three spaceborne DWLs mainly focus on the equatorial region.

https://doi.org/10.5194/amt-2020-202
Preprint. Discussion started: 29 June 2020

Atmospheric Measurement Techniques Discussions

As is mentioned in Introduction, Zhang et al., (2019) illustrate that the uncertainty of wind observations would increases of about 0.18 and 0.69 m/s in the troposphere and the stratosphere respectively as 20 $mW \cdot m^{-2} \cdot sr^{-1} \cdot nm^{-1}$ of SBR increases. Statistics illustrate that the averaged SBR of the three spaceborne DWLs are 20.99, 60.68, and 76.36 $mW \cdot m^{-2} \cdot sr^{-1} \cdot nm^{-1}$ respectively. The quantile statistics of SBR is presented in Table 1, which means that the corresponding percentages of the grids (the earth is divided into 1°×1° grid) of which the SBR will be smaller than the values listed in the first line of Table 1.

Table 1. Quantiles of SBR received by spaceborne DWLs operate in the three orbits.

Quantile (%)		20	40	50	60	70	80	90	100
SBR ($mW \cdot m^{-2} \cdot sr^{-1} \cdot nm^{-1}$)	Orbit 18:00	0	0	0	15.97	31.48	44.37	62.90	171.44
	Orbit 15:00	10.15	62.19	75.23	81.12	84.61	87.59	90.35	240.70
	Orbit 12:00	45.18	75.09	82.87	89.01	94.16	98.79	105.77	273.61

Figure 1 and Table 1 indicate that the spaceborne DWLs operate on the two new orbits would receive larger SBR compared with the sun-synchronous dawn-dusk orbit, which would lead to larger uncertainty of wind observations as is shown in the following subsection.

4.2 Uncertainties of wind observations based on the instrument parameters of Aeolus

Assuming the instrument parameters of the two new spaceborne DWLs were set to be the same as those of Aeolus, the profiles of wind observation uncertainties were derived as is shown in Fig. 3, which was obtained from the spaceborne DWLs simulation system using the 10 ° latitude-averaged SBR shown in Fig. 2, for whose contour lines illustrated that the distributions of SBR were nearly horizontal to latitude. Each subgraph in Fig. 3 was obtained based on 18 wind uncertainty profiles.

Figure 3 illustrates that the wind observation accuracy can meet the accuracy requirements of ESA in most bins of most latitudes in the troposphere and stratosphere even when the instrument parameters of the three spaceborne DWLs are the same as those of Aeolus. The bins of which uncertainty are beyond the requirements of ESA mostly located in the upper layer of troposphere and stratosphere. In addition, the accuracy of wind observations in the PBL is relatively low, which basically cannot meet the requirements of ESA. In fact, the Mie channel is mostly used for wind observations in the PBL, which are of higher accuracy. It is meaningless to study the wind observation accuracy of the Rayleigh channel in the PBL, the accuracy of the Rayleigh channel in the PBL is not considered in the following of this paper. As the LTANs of orbits get closer to noon, the wind observation uncertainty gradually increases, as the number of bins of which accuracy cannot meet the requirements of ESA. For the bins of troposphere and stratosphere, about 88.01% of the bins of Aeolus can meet the accuracy requirements of ESA, the percentages are 72.51% for the orbit of 15:00 and 66.37% for the orbit of 12:00. The averaged uncertainties of the three spaceborne DWLs in troposphere and stratosphere are shown in Table 2, which illustrates that the increments in wind

https://doi.org/10.5194/amt-2020-202
Preprint. Discussion started: 29 June 2020

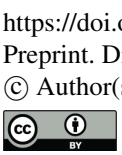

Atmospheric Measurement Techniques Discussions

observation uncertainties caused by the increments of SBR of new orbits range about from 0.3 to 0.4 m/s and from 0.9 to 1.4 m/s in troposphere and stratosphere respectively.

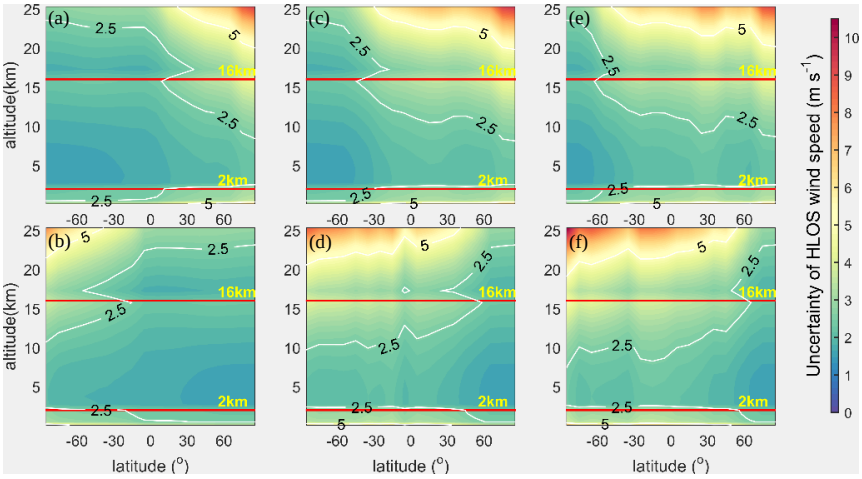

Figure 3. The zonal distributions of wind uncertainty observed by the three spaceborne DWLs operated on the three orbits of which the instrument parameters are the same as those of Aeolus. The contours show the accuracy requirements of ESA. The correspondence relationship between the subgraphs and orbits, seasons is consistent with Fig. 2.

Table 2. The averaged wind observation uncertainties of the three spaceborne DWLs in troposphere and stratosphere.

Local Time of Ascending Node		18:00	15:00	12:00
Uncertainty (m/s)	Troposphere	2.04	2.31	2.41
	Stratosphere	3.13	4.04	4.36

4.3 Distributions of required laser pulse energy

In order to make the accuracy of two new spaceborne DWLs to reach the specific accuracy level, the required laser pulse energy was obtained using the method mentioned in Subsect. 3.3. According to Eq. (11), the required energy is determined by temperature, pressure, wind uncertainty, and SBR, thus the required laser pulse energy is different in different bins. Therefore, the laser pulse energy of the spaceborne DWLs should be determined by the statistics of the profiles of required energy.

Supposed that the wind observation accuracy of the two new spaceborne DWLs is required to reach the accuracy level of Aeolus, which can be used for joint observations of the three satellites. Using the method mentioned in Subsect. 3.3, the global distributions of profiles of required laser pulse energy are derived and illustrated in Fig. 4.

Figure 4 illustrates that for most bins of the two new spaceborne DWLs, it is necessary to increase the laser pulse energy if the accuracy of the wind observation is expected to reach the accuracy level of Aeolus. Especially in the equatorial region, higher laser pulse energy is needed. The large differences of SBR in the equatorial region between the two new spaceborne DWLs and Aeolus can account for this phenomenon as Fig. 2 indicates.

https://doi.org/10.5194/amt-2020-202
Preprint. Discussion started: 29 June 2020

Atmospheric Measurement Techniques Discussions

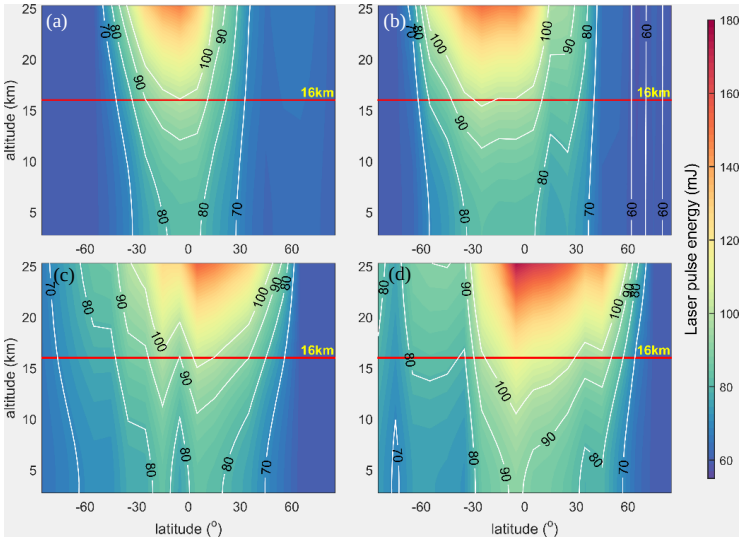

Figure 4. Global distributions of the required laser pulse energy in troposphere and stratosphere to make the wind observation accuracy of two new spaceborne DWLs reach the accuracy level of Aeolus. Figs. 4(a, c) and 4(b, d) denote the sun-synchronous orbit with LTANs of 15:00 and 12:00 respectively. The upper panels denote the distributions in summer, and the lower panels denote the distributions in winter.

Statistics reveal that the averaged values of required laser pulse energy in Fig. 4 are 72.00 and 85.03 mJ in the troposphere and stratosphere respectively for the 15:00 orbit, and 76.28 and 93.53 mJ in the troposphere and stratosphere for the 12:00 orbit respectively. The quantiles of the required energy of the two spaceborne DWLs are shown in Table 3 which means that the corresponding percentages of the bins whose accuracy will reach the accuracy level of Aeolus once the laser pulse energy equals to the specific values.

Table 3. Quantiles of the required laser pulse energy of the two new spaceborne DWLs to reach the accuracy level of Aeolus.

Quantile (%)		20	40	50	60	70	80	90	100
Required energy	Orbit 15:00	61.21	66.61	71.68	76.49	80.67	85.09	94.65	154.45
(mJ)	Orbit 12:00	62.26	74.69	78.27	82.11	86.60	92.27	105.21	175.53

Another potential application of the added spaceborne DWLs is to enlarge the global wind observation coverage to improve the forecast results of NWP. Once the wind observation accuracy meets the requirements of ESA, it is supposed to have positive impact on NWP results. The distributions of required laser pulse energy of the three orbits to meet the accuracy requirements of ESA are derived using the method mentioned in Subsect. 3.3 and illustrated in Fig. 5.

Figure 5 illustrates that the wind observation uncertainties of most bins can meet the accuracy requirements of ESA for the three spaceborne DWLs with the laser pulse energy of 60 mJ. Higher energy is needed mostly in the upper level of troposphere and stratosphere near the regions close to Antarctic and Arctic circles. The closer the orbital LTAN is to noon, the averaged values of the required laser energy will become larger. Statistics show that the averaged values of required energy are 41.76 and 28.69 mJ in the troposphere and stratosphere for Aeolus, 52.42 and 44.57 mJ in the troposphere and stratosphere

https://doi.org/10.5194/amt-2020-202
Preprint. Discussion started: 29 June 2020

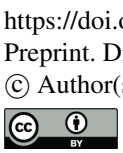

Atmospheric Measurement Techniques Discussions

for the 15:00 orbit, and 56.05 and 49.73 mJ in the troposphere and stratosphere for the 12:00 orbit respectively. The quantiles of the required energy of the three spaceborne DWLs are shown in Table 4. The statistics and Table 4 illustrate that not too larger laser energy is required to meet ESA's accuracy requirements for wind observations. Even if the instrument parameters of the spaceborne DWLs are consistent with that of Aeolus, the wind observation accuracy of above 60% of bins can basically meet the accuracy requirements of ESA.

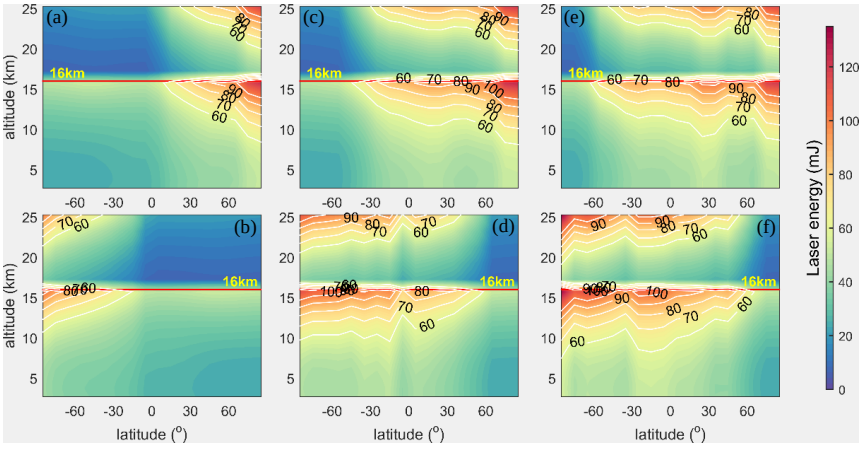

Figure 5. Global distributions of the required laser pulse energy in troposphere and stratosphere to reach the accuracy requirements of ESA. The correspondence relationship between the subgraphs and orbits, seasons is consistent with Fig. 2.

Table 4. Quantiles of the required laser pulse energy of the three spaceborne DWLs to meet the accuracy requirements of ESA.

Quantile (%)		20	40	50	60	70	80	90	100
Required energy (mJ)	Orbit 18:00	24.35	31.02	35.17	39.86	44.69	51.00	63.91	122.63
	Orbit 15:00	31.57	44.65	47.39	51.86	57.53	67.66	82.07	125.19
	Orbit 12:00	36.64	47.37	50.96	55.75	62.35	72.58	85.60	135.23

4.4 Uncertainties of wind observations based on new instrument parameter proposal

In Subsect. 4.3, the zonal profiles of required laser pulse energy were derived for different purposes. In order to offer a feasible proposal for the laser pulse energy of the new spaceborne DWLs, the percentages of bins that can meet the specific accuracy requirements when the laser energy reaches a certain value were figured out, as is shown in Table 5.

Table 5 illustrates that the percentages of bins that meet the specific accuracy requirements will become larger with higher laser pulse energy. However, assuming the laser energy increases by the same amount each time, the increments of the percentages decrease. According to the current technology, the technical difficulty will increase a lot for each small increment in the laser energy of spaceborne DWLs. Considering the accuracy requirements of ESA and accuracy level of Aeolus, while taking the existing technical level into account, the laser energy of the two new spaceborne DWLs is set to 80 mJ. In this way,

https://doi.org/10.5194/amt-2020-202
Preprint. Discussion started: 29 June 2020

Atmospheric Measurement Techniques Discussions

at least half of the bins can reach the accuracy level of Aeolus, and the percentages of bins that meet the ESA's accuracy requirements will be higher than 85% for the two new spaceborne DWLs as Table 5 illustrates.

Table 5. Percentages of bins which will meet the specific accuracy requirements with certain laser pulse energy for spaceborne DWLs.

Accuracy requirements		Laser pulse energy (mJ)					
		50	60	70	80	90	100
ESA (%)[a]	Orbit 18:00	78.80	88.01	92.98	95.76	97.81	98.98
	Orbit 15:00	55.99	72.51	82.16	89.33	94.30	97.81
	Orbit 12:00	47.08	66.37	78.07	86.40	92.54	96.05
Aeolus (%)[b]	Orbit 15:00	0	19.44	46.78	68.57	85.96	92.98
	Orbit 12:00	0	16.67	30.85	54.39	76.75	87.28

[a] The percentage of bins which will meet the accuracy requirements of ESA when the laser energy reaches the specific value.

[b] The percentage of bins which will reach the accuracy level of Aeolus in the corresponding bins when the laser energy reaches the specific value.

Provided that the three spaceborne DWLs operate on the sun-synchronous orbits shown in Fig. 1. The instrument parameters of Aeolus keep unchanged. As to the two new Aeolus-type spaceborne DWLs, the other instrument parameters are set as same as those of Aeolus except for the laser pulse energy of 80 mJ. The wind observation uncertainty distributions of the three spaceborne DWLs is derived as is shown in Fig. 6.

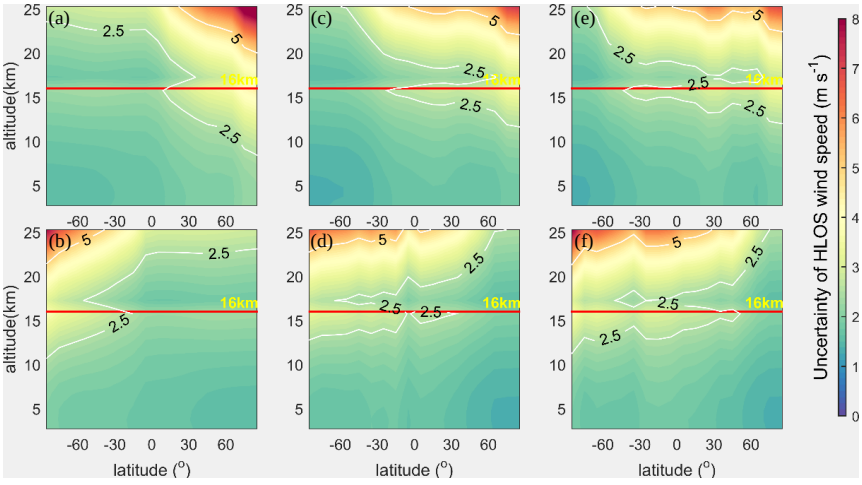

Figure 6. The zonal distributions of wind observation uncertainties of the three spaceborne DWLs with new instrument parameters, of which the laser energy of Aeolus is 60 mJ, and the laser energy of the two new Aeolus-type spaceborne DWLs is 80 mJ. The correspondence relationship between the subgraphs and orbits, seasons is consistent with Fig. 2.

The contour lines in Fig. 6 (c, d) and (e, f) illustrate that most of bins of the two new spaceborne DWLs could meet the accuracy requirements of ESA with laser pulse energy of 80 mJ. As Table 5 shows that about 89.33% of the bins of the

https://doi.org/10.5194/amt-2020-202
Preprint. Discussion started: 29 June 2020


Atmospheric Measurement Techniques Discussions

spaceborne DWL operating on the orbit with LTAN of 15:00 could reach the accuracy requirements, and the percentage is 86.40% for the orbit of 12:00. The comparisons between Fig. 6 (c, d) (e, f) and (a, b) indicate that the wind observation accuracy of the three spaceborne DWLs operating on the three sun-synchronous orbits is of consistence using the instrument parameter proposal provided in this paper. The accuracy of wind observations of the two new spaceborne DWLs with laser pulse energy of 80 mJ is slightly higher than that of Aeolus in the troposphere, and lower than that of Aeolus in the stratosphere. The averaged uncertainties of the three spaceborne DWLs operating on the three orbits in troposphere and stratosphere are shown in Table 6. And Table 6 illustrates that the differences of the averaged uncertainties range from 0.06 to 0.33 m/s among the three spaceborne DWLs, which also demonstrates the consistence in wind observation accuracy. Comparisons among Fig. 6(c-f) and Fig. 3(c-f) illustrate that, as for the two new spaceborne DWLs, when the laser energy increases from 60 mJ to 80 mJ, the observation accuracy could be improved significantly.

Table 6. The averaged wind observation uncertainties of the three spaceborne DWLs with the proposed instrument parameters.

Local Time of Ascending Node (LTAN)		18:00	15:00	12:00
Uncertainty	Troposphere	2.04	1.91	1.97
(m/s)	Stratosphere	3.13	3.21	3.46

5 Summary and conclusions

The successful launch of Aeolus is significant for people to observe the global wind field. Aeolus operates on the sun-synchronous dawn-dusk orbit to minimize the impact of SBR on the accuracy of wind observations. If the future spaceborne DWLs operate on other sun-synchronous orbits for their specific observation purposes, the received SBR may become larger which would lead to higher observation uncertainties. In this paper, the influence of the LTAN crossing of sun-synchronous on the wind observation accuracy of Aeolus-type spaceborne DWLs was studied. And increasing laser pulse energy of spaceborne DWLs was used to lower the observation uncertainties. Furthermore, the method to quantitatively design laser pulse energy to meet the specific accuracy requirements was also studied.

Assuming two new Aeolus-type spaceborne DWLs operate on the sun-synchronous orbits with LTAN of 15:00 and 12:00. The global distributions of SBR illustrate that the increments of averaged SBR range from 39 to 56 $mW \cdot m^{-2} \cdot sr^{-1} \cdot nm^{-1}$ on the two new orbits compared to that of Aeolus under clear skies, which will lead to the averaged uncertainty increment of 0.3 to 0.4 m/s in the troposphere and 0.9 to 1.4 m/s in the stratosphere, respectively. And the statistics show that 88.01% of the bins of Aeolus can meet the accuracy requirements of ESA. For the two new spaceborne DWLs, the percentages are 72.51% for the orbit of 15:00 and 66.37% for the orbit of 12:00.

To quantitatively design the required laser pulse energy of the new spaceborne DWLs to meet specific accuracy requirements, i.e. to meet the accuracy requirements of ESA, or to reach the similar accuracy level of Aeolus, the relationship

https://doi.org/10.5194/amt-2020-202
Preprint. Discussion started: 29 June 2020

Atmospheric Measurement Techniques Discussions

between SNR and the uncertainty of response function of Rayleigh channel is established based on some assumption and simplifications, which is proven of wide feasibility by simulation experiments as is shown in Appendix. Finally, the method to derive the required laser energy according to accuracy requirements is proposed.

If the accuracy requirements of the two new spaceborne DWLs are to reach the accuracy level of Aeolus, the global distributions of the derived laser pulse energy demonstrate that it is necessary to increase the laser pulse energy. If the purpose of the new spaceborne DWLs is to improve the results of NWP, the wind observation accuracy should be meet the accuracy requirements of ESA. It is demonstrated that the wind observation uncertainty of most bins can meet the requirements even when the laser pulse energy of the two new spaceborne DWLs is set as the same as that of Aeolus. Considerations are given to both of reaching the accuracy level of Aeolus and improving the forecast results of the NWP, taking existing technical level of spaceborne DWLs into account, the laser pulse energy of two new spaceborne DWLs is set to 80 mJ, while other parameters are the same as those of Aeolus. Based on the parameter proposal, at least half of the bins can reach the accuracy level of Aeolus, and the percentages of bins that meet the ESA's accuracy requirements will be higher than 85% for the two new spaceborne DWLs. The differences of the averaged observation uncertainties are between 0.06 and 0.33 m/s among the three spaceborne DWLs, which illustrate of consistence in observation accuracy.

The essence of lowering the wind observation uncertainties of spaceborne DWLs by increasing the laser pulse energy is to increase the SNR of received signal. Other methods can be used to improve the SNR of received signal, such as enlarging the telescope aperture or reducing vertical resolution. Once the quantitative relationship between these instrument parameters and the SNR is established, we can also quantitatively adjust these parameters according to our accuracy requirements.

Appendix

To build the relationship between laser pulse energy and uncertainties of wind observations for Aeolus-type spaceborne DWLs, we derived the relationship between the response function and SNR of Rayleigh channel, firstly. According to Eqs. (3) and (4), the uncertainty of response function of Rayleigh channel can be written as

$$\begin{aligned}\sigma_{R_{ATM}} &= \frac{2}{(N_A+N_B)^2}\sqrt{N_B^2\left(N_A+N_{S,A}+N_{noise}^2\right)+N_A^2\left(N_B+N_{S,B}+N_{noise}^2\right)} \\ &= \frac{2}{(N_A+N_B)^2}\sqrt{N_AN_B(N_A+N_B)+N_{noise}^2(N_A^2+N_B^2)+N_A^2N_{S,B}+N_B^2N_{S,A}}\end{aligned} \tag{A1}$$

According to Eq. (6), the SNR of Rayleigh channel for spaceborne DWLs can be expressed as

$$\begin{aligned}SNR_{Ray} &= \frac{N_A+N_B}{\sqrt{N_A+N_B+N_{S,A}+N_{S,B}+2N_{noise}^2}} \\ &= \frac{(N_A+N_B)^2}{\sqrt{(N_A+N_B)^2(N_A+N_B)+(N_A+N_B)^2(N_{S,A}+N_{S,B})+2N_{noise}^2(N_A+N_B)^2}} \\ &= \frac{(N_A+N_B)^2}{\sqrt{(N_A^2+N_B^2+2N_AN_B)(N_A+N_B)+(N_A^2+N_B^2+2N_AN_B)(N_{S,A}+N_{S,B})+2N_{noise}^2(N_A^2+N_B^2+2N_AN_B)}} \\ &= \frac{(N_A+N_B)^2}{\sqrt{2N_AN_B(N_A+N_B)+2N_{noise}^2(N_A^2+N_B^2)+N_A^2N_{S,B}+N_B^2N_{S,A}+N_A^2N_{S,A}+N_B^2N_{S,B}+(N_A^2+N_B^2)(N_A+N_B)+4N_{noise}^2N_AN_B+2N_AN_B(N_{S,A}+N_{S,B})}}\end{aligned} \tag{A2}$$

https://doi.org/10.5194/amt-2020-202
Preprint. Discussion started: 29 June 2020

Atmospheric Measurement Techniques Discussions

For useful signal N_A and N_B received by Rayleigh channel, when the absolute values of HLOS wind components are not large, the assumption $N_A \approx N_B$ can be made, then

$$N_A^2 N_{S,B} + N_B^2 N_{S,A} + N_A^2 N_{S,A} + N_B^2 N_{S,B} \approx 2\left(N_A^2 N_{S,B} + N_B^2 N_{S,A}\right) \tag{A3}$$

$$(N_A^2 + N_B^2)(N_A + N_B) \approx 2N_A N_B (N_A + N_B) \tag{A4}$$

$$4N_{noise}^2 N_A N_B \approx 2N_{noise}^2 (N_A^2 + N_B^2) \tag{A5}$$

$$2N_A N_B \left(N_{S,A} + N_{S,B}\right) \approx 2\left(N_A^2 N_{S,A} + N_B^2 N_{S,A}\right) \tag{A6}$$

After the assumption and simplifications,

$$SNR_{Ray} \approx \frac{(N_A+N_B)^2}{2\sqrt{N_A N_B (N_A+N_B)+N_{noise}^2 (N_A^2+N_B^2)+N_A^2 N_{S,B}+N_B^2 N_{S,A}}} = \frac{1}{\sigma_{R_{ATM}}} \tag{A7}$$

As is the equations derivation process shown in Subsect. 3.2, the relationship between SNR and uncertainty of response function shown in Eq. (A7) is the basis to derive the relationship between laser pulse energy and wind observation uncertainty shown in Eqs. (10) and (11). However, Eq. (A7) is derived through assumption and simplifications, especially the assumption $N_A \approx N_B$, of which the values may be of large differences when the absolute values of HLOS wind speed are large. To test the correctness of Eq. (A7) in the actual atmosphere with variable wind speed, we verified the equation using reanalysis data, aerosol optical parameters database LIVAS and surface albedo database. The verification process is shown in Fig. A1.

The reanalysis data is obtained from the 20th Century Reanalysis Project (Compo *et al.*, 2011). In the validation experiment, the monthly averaged 24 level profiles of temperature, pressure, u- and v-component wind with 1°×1° spatial resolution are obtained from the reanalysis data. In this study, the reanalysis data for June 2015 and December 2015 are used as the atmospheric condition in summer and winter respectively. As is shown in Fig. A1, the verification process of Eq. (A7) can be described as follows:

(1) The off-nadir points of spaceborne DWLs are obtained using orbit simulation software based on the orbit information of spaceborne DWLs.

(2) The profiles of temperature, pressure, wind speed, aerosol optical parameters, and surface albedo are interpolated into the off-nadir points.

(3) The SBR of the off-nadir points are derived using RTM libRadtran with the inputs provided in step (2).

(4) The profile values of N_A, N_B and $N_{S,A}$, $N_{S,B}$ are figured out using spaceborne DWL simulation system mentioned in Subsect. 2.2 with the inputs of SBR and atmospheric conditions of off-nadir points.

(5) The values of $\sigma_{R_{ATM}}$ and SNR_{Ray} are obtained using Eqs. (3), (4), and (6). In this study, the value of N_{noise} is assumed to be zero, which means the dark current of the detectors on Rayleigh channel is negligible.

https://doi.org/10.5194/amt-2020-202
Preprint. Discussion started: 29 June 2020

Atmospheric Measurement Techniques Discussions

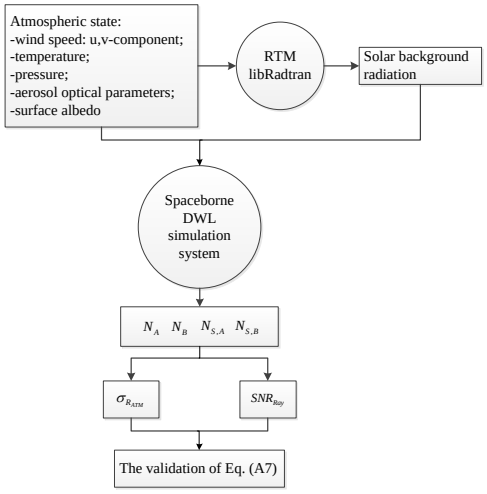

Figure A1. The verification process of Eq. (A7).

The scatters of $\sigma_{R_{ATM}}$ and $1/SNR_{Ray}$ are plotted to verify the accuracy of Eq. (A7), as is shown in Fig. A2. The spatial resolution of the reanalysis data is 1°×1°, so the earth is divided into 1°×1° grid during the verification process, and one off-nadir point in each grid is selected as the verification point. Considering the SBR in summer and winter, and excluding some grid points with invalid data, a total of 28460 profiles are used in this verification. Each profile contains 24 bins, the verification uses 683040 scattered points.

In the verification, the HLOS wind components derived from u- and v-wind component ranges from -73.02 to 33.14 m/s. Figure A2 illustrate that the scatter plot between reciprocal SNR and uncertainty of response function of Rayleigh channel is very close to the line $y = x$ with little residuals, which demonstrates that the assumption and simplifications used in deriving the relationship between the laser pulse energy and the uncertainty of wind observation are reasonable, and Eq. (A7) is of wide feasibility in the real atmosphere.

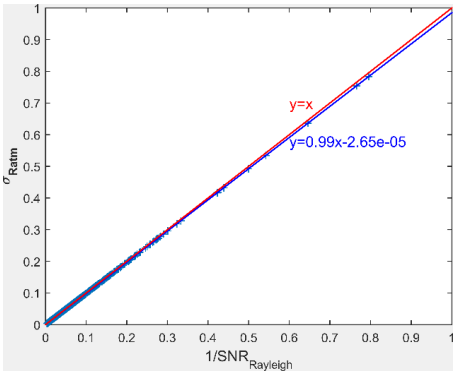

Figure A2. The scatter plot between reciprocal SNR and uncertainty of response function of Rayleigh channel and their first order fitting relationship.

https://doi.org/10.5194/amt-2020-202
Preprint. Discussion started: 29 June 2020

Atmospheric Measurement Techniques Discussions

The variables used in the verification of Eq. (A7) can be also used in the verification of Eq. (11). The variable of $\partial v_{HLOS}/\partial R_{ATM}$ is also need, which is the function of temperature and pressure, and can be obtained through a pre-calculated lookup table. The verification results of Eq. (11) are shown in Fig. A3.

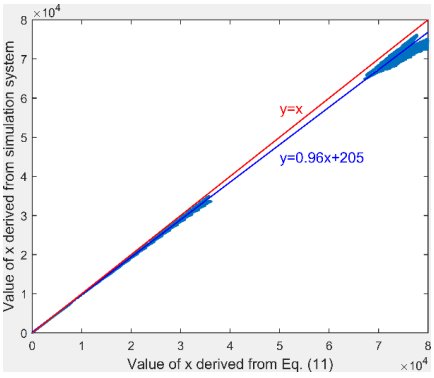

Figure A3. The scatter plot of the values of $\boldsymbol{x}$ which are derived from Eq. (11) and simulation system which is the sum of $\boldsymbol{N_A}$ and $\boldsymbol{N_B}$ respectively.

As is shown in Fig. A3, the fitting line of the scatter plot of value x derived from Eq. (11) and simulation system is very close to the line $y = x$. Furthermore, the residuals between the scattered points and the fitted line are very small, which indicate the wide feasibility of Eq. (11). In addition, it is noteworthy that the scattered points of Fig. A3 are mostly located below the line $y = x$, which indicates that the value of x calculated by Eq. (11) is smaller than the actual value. According to Subsect. 3.4, the laser pulse energy is derived based on the equation $E_{new}/E_{Aeolus} \approx x2/x1$. And $x1$ is obtained from simulation system, which is regarded to be close to real value. The smaller $x2$ may lead to smaller E_{new}, which is about 0.96 times to the real value.

Code and Data availability. The codes in this article are mainly compiled using matlab and are available upon request from the first author by email, zhang01020@hotmail.com. The databases used in this paper include: OMI database, which provided the latitude-averaged temperature, pressure, and ozone, can be accessed via anonymous ftp from toms.gsfc.nasa.gov/pub/LLM_climatology; LIVAS database, providing the golabl aerosol optical properties with 1°×1° grid, offered by Dr. V. Amiridis from Institude for space applications and remote sensing, National observatory of Athens, and can be assessed from http://lidar.space.no a.gr:8080/livas/; the global LER database is available upon request from the authors, Dr. R. B. A. Koelemeijer from Air Research Laboratory, National Institute of Public Health and the Environment, robert.koelemeijer@rivm.nl; and the reanalysis data of 20th Century Reanalysis provided by the NOAA/OAR/ESRL PSD, Boulder, Colorado, USA, from their Web site at https://www.esrl.noaa.gov/psd/.

Author contributions. CZ, XS, and WL designed the studies; CZ built the simulation systems, performed the computation and analysis, and wrote the paper text; YS, ND, and SL provided important information on data delivery and processing. All authors engaged in discussions on studies, interpretation of results, as well as contribution to the finalization of the paper text.

Competing interests. The authors declare that they have no conflict of interest.

Acknowledgements. Thanks for the helpful discussions provided by Dr. Karsten Schmidt from DLR, Dr. Gert-Jan Marseille and Dr. Ad Stoffelen from Royal Netherlands Meteorological Institute in the building simulation system of Aeolus-type spaceborne DWLs. Thanks for the suggestions provided by Dr. Claudia Emde in running the libRadtran.

Financial support. This research was supported by National Natural Science Foundation of China (NSFC) (41575020).

References:

Amiridis, V., Marinou, E., Tsekeri, A., Wandinger, U., Schwarz, A., Giannakaki, E., Mamouri, R., Kokkalis, P., Binietoglou, I., Solomos, S., Herekakis, T., Kazadzis, S., Gerasopoulos, E., Proestakis, E., Kottas, M., Balis, D., Papayannis, A., Kontoes, C., Kourtidis, K., Papagiannopoulos, N., Mona, L., Pappalardo, G., Le Rille, O. and Ansmann, A.: LIVAS: a 3-D multi-wavelength aerosol/cloud database based on CALIPSO and EARLINET, Atmos. Chem. Phys., 15(13), 7127-7153, https://doi.org/10.5194/acp-15-7127-2015, 2015.

Baars, H., Geiß, A., Wandinger, U., Herzog, A., Engelmann, R., Bühl, J., Radenz, M., Seifert, P., Althausen, D., Heese, B., Ansmann, A., Martin, A., Leinweber, R., Lehmann, V., Weissmann, M., Cress, A., Filioglou, M., Komppula, M. and Reitebuch, O.: First results from the German CAL/VAL activities for Aeolus, The 29th International Laser Radar Conference, Hefei, China, 2019.

Compo, G. P., Whitaker, J. S., Sardeshmukh, P. D., Matsui, N., Allan, R. J., Yin, X., Gleason, B. E., Vose, R. S., Rutledge, G., Bessemoulin, P., Brönnimann, S., Burnet, M., Crouthamel, R. I., Grant, A. N., Groisman, P. Y., Jones, P. D., Kruk, M. C., Kruger, A. C., Marshall, G. J., Maugeri, M., Mok, H. Y., Nordli, Ø., Ross, T. F., Trigo, R. M., Wang, X. L., Woodruff, S. D. and Worley, S. J.: The Twentieth Century Reanalysis Project, Q. J. Roy. Meteor. Soc., 137(654), 1-28, https://doi.org/10.1002/qj.776, 2011.

Emde, C., Buras-Schnell, R., Kylling, A., Mayer, B., Gasteiger, J., Hamann, U., Kylling, J., Richter, B., Pause, C., Dowling, T. and Bugliaro, L.: The libRadtran software package for radiative transfer calculations (version 2.0.1). Geosci. Model Dev., 9(5), 1647-1672, https://doi.org/10.5194/gmd-9-1647-2016, 2016.

Flamant, P., Cuesta, J., Denneulin, M., Dabas, A. and Huber, D.: ADM-Aeolus retrieval algorithms for aerosol and cloud products, Tellus A, 60(2), 273-286, https://doi.org/10.1111/j.1600-0870.2007.00287.x, 2008.

Flesia, C. and Korb, C. L.: Theory of the double-edge molecular technique for Doppler lidar wind measurement, Appl. Opt., 38(3), 432-440, 1999.

Hasinoff, S. W., Durand, F. and Freeman, W. T.: Noise-Optimal Capture for High Dynamic Range Photography, Proceedings of the IEEE Computer Society Conference on Computer Vision and Pattern Recognition, Los Alamitos, 553-560, https://doi.org/10.1109/CVPR.2010.5540167, 2010.

Heliere, A., Bezy, J. L., Bensi, P. and Ingmann, P.: System definition of the ESA Earth Explorer WALES mission, Sensors, Systems, and Next-Generation Satellites VI, Crete, Greece, 24-32, 2002.

Ishii, S., Baron, P., Aoki, M., Mizutani, K., Yasui, M., Ochiai, S., Sato, A., Satoh, Y., Kubota, T., Sakaizawa, D., Oki, R., Okamoto, K., Ishibashi, T., Tanaka, T. Y., Sekiyama, T. T., Maki, T., Yamashita, K., Nishizawa, T., Satoh, M. and Iwasaki, T.: Feasibility study for future space-borne coherent Doppler wind lidar, Part 1: Instrumental Overview for Global Wind Profile Observation, J. Meteorol. Soc. Jpn., 95(5), 301-317, https://doi.org/10.2151/jmsj.2017-017, 2017.

Koelemeijer, R., de Haan, J. F. and Stammes, P.: A database of spectral surface reflectivity in the range 335-772 nm derived from 5.5 years of GOME observations, J. Geophy. Res.-Atmos., 108(D2), 171-181, https://doi.org/10.1029/2002JD002429, 2003.

Liu, Z., Hunt, W., Vaughan, M., Hostetler, C., Mcgill, M., Powell, K., Winker, D. and Hu, Y.: Estimating random errors due to shot noise in backscatter lidar observations, Appl. Opt., 45(18), 4437-4447, https://doi.org/10.1364/AO.45.004437, 2006.

Ma, Z., Riishojgaard, L. P., Masutani, M., Woollen, J. S. and Emmitt, G. D.: Impact of different satellite wind lidar telescope configurations on NCEP GFS forecast skill in observing system simulation experiments, J. Atmos. Ocean. Tech., 32(3), 478-495, https://doi.org/10.1175/JTECH-D-14-00057.1, 2015.

Marseille, G. J. and Stoffelen, A.: Simulation of wind profiles from a space-borne Doppler wind lidar. Q. J. Roy. Meteor. Soc., 129(594A), 3079-3098, https://doi.org/10.1256/003590003769682183, 2003.

Marseille, G., Stoffelen, A. and Barkmeijer, J.: Impact assessment of prospective spaceborne Doppler wind lidar observation scenarios, Tellus A, 60(2), 234-248, https://doi.org/10.1111/j.1600-0870.2007.00289.x, 2008.

Masutani, M., Woollen, J. S., Lord, S. J., Emmitt, G. D., Kleespies, T. J., Wood, S. A., Greco, S., Sun, H. B., Terry, J., Kapoor, V., Treadon, R. and Campana, K. A.: Observing system simulation experiments at the National Centers for Environmental Prediction, J. Geophys. Res.-Atmos., 115(D7), https://doi.org/10.1029/2009JD012528, 2010.

Mcpeters, R., Kroon, M., Labow, G., Brinksma, E., Balis, D., Petropavlovskikh, I., Veefkind, J. P., Bhartia, P. K. and Levelt, P. F.: Validation of the Aura Ozone Monitoring Instrument total column ozone product, J. Geophys. Res.-Atmos., 113 (15). https://doi.org/10.1029/2007JD008802, 2008.

https://doi.org/10.5194/amt-2020-202
Preprint. Discussion started: 29 June 2020

Nakajima, T. Y., Imai, T., Uchino, O. and Nagai, T.: Influence of daylight and noise current on cloud and aerosol observations by spaceborne elastic scattering lidar. Appl. Opt., 38(24), 5218-28, https://doi.org/10.1364/AO.38.005218, 1999.

Paffrath, U.: Performance assessment of the Aeolus Doppler wind lidar prototype, Doctor of Engineering, Ludwig-Maximilians-Universität München, 2006.

Reitebuch, O., Paffrath, U. and Leike, I.: ATBD: ADM-Aeolus Level 1B Product, European Space Agency, 2006.

Rennie, M.: CCN6 results: further Chain-of-Processors testing of L2B results and testing of CCN6 L2B processor algorithm updates, European Centre for Medium-Range Weather Forecasts, 2017.

Stoffelen, A., Marseille, G. J., Bouttier, F., Vasiljevic, D., de Haan, S. and Cardinali, C.: ADM-Aeolus Doppler wind lidar Observing System Simulation Experiment, Q. J. Roy. Meteor. Soc., 132(619B), 1927-1947, https://doi.org/10.1256/qj.05.83, 2006.

Stoffelen, A., Pailleux, J., Kallen, E., Vaughan, J. M., Isaksen, L., Flamant, P., Wergen, W., Andersson, E., Schtberg, H., Culoma, A., Meynart, R., Endemann, M. and Ingmann, P.: The atmospheric dynamics mission for global wind field measurement, B. Am. Meteorol. Soc., 86(1), 73, https://doi.org/10.1175/BAMS-86-1-73, 2005.

Straume, A. G., Rennie, M., Isaksen, L., de Kloe, J., Marseille, G. J., Stoffelen, A., Flament, T., Stieglitz, H., Dabas, A., Huber, D., Reitebuch, O., Lemmerz, C., Lux, O., Marksteiner, U., Weiler, F., Witschas, B., Meringer, M., Schmidt, K., Nikolaus, I., Geiss, A., Flamant, P., Kanitz, T., Wernham, D., von Bismarck, J., Bley, S., Fehr, T., Floberghagen, R. and Parrinello, T.: ESA's space-based Doppler wind lidar mission Aeolus first wind and aerosol product assessment results, The 29th International Laser Radar Conference, Hefei, China, 2019.

Sun, X. J., Zhang, R. W., Marseille, G. J., Stoffelen, A., Donovan, D., Liu, L. and Zhao, J.: The performance of Aeolus in heterogeneous atmospheric conditions using high-resolution radiosonde data, Atmos. Meas. Tech., 7(8), 2695-2717. https://doi.org/10.5194/amt-7-2695-2014, 2014.

Tan, D. G. H., Anderson, E., De Kloe, J., Marseille, G., Stoffelen, A., Poli, P., Denneulin, M., Dabas, A., Huber, D., Reitebuch, O., Flamant, P., Le Rille, O. and Nett, H.: The ADM-Aeolus wind retrieval algorithms, Tellus A, 60(2), 191-205. https://doi.org/10.1111/j.1600-0870.2007.00285.x, 2008.

Vahlbruch, H., Mehmet, M., Chelkowski, S., Hage, B., Franzen, A., Lastzka, N., Gossler, S., Danzmann, K. and Schnabel, R.: Observation of squeezed light with 10-dB quantum-noise reduction, Phys. Rev. Lett., 100(3), 033602, https://doi.org/10.1103/PhysRevLett.100.033602, 2008.

Zhang, C. L., Sun, X. J., Zhang, R. W. and Liu, Y. W.: Simulation and assessment of solar background noise for spaceborne lidar, Appl. Opt., 57(31), 9471-9479, https://doi.org/10.1364/AO.57.009471, 2018.

Zhang, C. L., Sun, X. J., Zhang, R. W., Zhao, S. J., Lu, W., Liu, Y. W. and Fan, Z. Q.: Impact of solar background radiation on the accuracy of wind observations of spaceborne Doppler wind lidars based on their orbits and optical parameters, Opt. Express, 27(12), A936-A952, https://doi.org/10.1364/OE.27.00A936, 2019.

https://doi.org/10.5194/amt-2020-202
Preprint. Discussion started: 29 June 2020

570 Zhang, R. W., Sun, X. J., Yan, W., Zhao, J., Liu, L., Li, Y., Zhang, C. L. and Zhou, J. H.: Simulation of frequency discrimination for spaceborne Doppler wind lidar (II): Study on the retrieval of atmospheric wind speed for Rayleigh channel based on Fabry-Perot interferometer, Acta Phys. Sin.-Ch. Ed., 63(14), 147-156. https://doi.org/10.7498/aps.63.140703, 2014.